UNIVERSITÀ DEGLI STUDI DI
MILANO-BICOCCA


Scuola di Scienze Matematiche Fisiche e Naturali
Corso di laurea Triennale in Fisica

# PROBING OPTICAL AND RADIO-LOUD AGN FRACTIONS : A COMPARATIVE ANALYSIS BETWEEN BCGs AND NON-BCGs SAMPLES at z $<$ 0.1

*Candidate:*
Andrea Maccarinelli

*Supervisor:*
Prof. Sebastiano Cantalupo

*Co-supervisors:*
Dott. Andrea Travascio

anno accademico 2022/2023

# Abstract

Brightest cluster galaxies (BCGs) are the most massive and luminous galaxies located near the center of relaxed, virialized, and undisturbed galaxy clusters in the local Universe ([1, 2]). According to several observational studies ([3, 4]), these objects experience a special formation process differing from general galaxy evolution.

Current theoretical models (e.g., [5, 6]) predict that dry mergers are the dominant mechanisms responsible for their mass assembly at $z < 1$. These objects are often observed to host a supermassive black hole (SMBH) in their center ([7]). The process of matter accretion into these SMBHs may release a large amount of energy, resulting in Active Galactic Nuclei (AGN). There are two primary modes in which SMBH accretion can occur: the so-called 'quasar mode' and the 'radio mode'. The quasar mode involves a high accretion rate of the SMBH via an optically- thick and geometrically-thin disk, with most of the energy being released in the form of radiation. In a radio mode scenario, the SMBH accretion of gas occurs at a low rate with an optically-thin and geometrically-thick disk configuration, releasing energy in the form of relativistic particles, i.e. radio jets. The latter is typically observed in BCGs [8].

The evolutionary processes of BCGs are still not fully understood, and there are no specific studies comparing the frequency of different types of AGN in BCGs with respect to other types of galaxies (e.g., [9]). The main scientific question guiding my thesis project is to investigate whether the different evolution of BCGs, coupled with their "special" environment, promotes the accretion of SMBHs in their centers compared to other types of galaxies in the local universe, at $z < 0.1$. To address this question, I analyzed a sample of BCGs within the redshift range of z = 0.02-0.1. This sample was derived from the combination of the Sloan Digital Sky Survey Data Release 7 (SDSS DR7 [10]) and the C4 BCGs catalogue produced by

[11, 12]. I utilized the flux measurements of optical emission lines i.e. $H\alpha$, [OIII], $H\beta$, [NII], and [SII] doublets estimated by the Max Planck Institute for Astrophysics and Johns Hopkins University ( MPA-JHU ) teams using the methods outlined in [13]. This allowed me to conduct a selection of optical AGN through the [NII]- and [SII]- BPT diagnostic diagrams [14]. Additionally, I conducted a cross-matching of the aforementioned catalogs with a dataset obtained from [15], where the spectroscopic sample of the SDSS DR2 was cross-correlated with catalogs of galaxies observed from the National Radio Astronomy Observatory (NRAO) Very Large Array (VLA) Sky Survey (NVSS; [16]) and the Faint Images of the Radio Sky at Twenty centimeters (FIRST) survey [17]. Using this new catalog of BCGs probed with these radio surveys, I was able to select the BCGs that exhibit radio loudness. Following this classification, I finally estimated the fraction of BCGs classified as Optical and Radio Loud AGN. Subsequently, I derived these fractions for a sample of non-BCG selected galaxies using the same procedure employed to obtain the BCG catalog.

These analyses reveal that BCGs exhibit a higher fraction of Optical AGN $\sim 50\%$ compared to the non-BCG sample, which shows a percentage of $\sim 21\%$, consistent with the results found by [18]. Simultaneously, the analysis of Radio Loud emissions indicates that BCGs are more inclined to host Radio Loud Activity, with a fraction of $\sim 12\%$. This fraction is found to be 20 times higher than the fraction observed in the non-BCG sample of selected galaxies, which is $\sim 0.6\%$.

In conclusion, these results demonstrate that BCGs are more likely to host optical AGN activity and radio-loud emission compared to other types of galaxies. This suggests that their privileged position facilitates frequent accretion of SMBHs in both accretion modes. Previous studies (e.g. [11, 19, 20]) have already shown a prevalence of radio AGN among the BCG population in the local Universe. On the other hand, few studies (e.g., [9, 11]) have attempted to compare the distribution of BCGs in BPT diagrams to that of normal galaxies. The fact that the fraction of AGN is greater for special galaxies is important to understand the nature of these objects. Future studies will aim to test the results obtained with this sample and to understand if this higher fraction is specifically driven by differences in properties between BCGs and non-BCGs, such as mass, star formation rate, metallicity, and kinematics.

# Contents

# Chapter 1

# Introduction

## 1.1 The Active Galactic Nuclei: Quasar vs. Radio Accretion Modes

Active galaxies constitute a distinctive class characterized by an intensely energetic source at their center, known as an Active Galactic Nucleus (AGN). Since the first observation of an active galaxy in the early 1900s [21], numerous studies have been conducted on this intriguing category of galaxies. To this day, efforts persist in unraveling the nature and role of active galaxies within the broader context of galactic formation and evolution.

Research in this field has demonstrated that the intense radiation must emanate from a compact region, with a spatial dimension not exceeding 100 parsecs. This estimation was derived from the temporal variability observed in some of these sources [22]. Additionally, it has been noted that AGNs exhibit luminosity variations of over 50% within timescales ranging from days to years. Such fluctuations can only be explained if a substantial portion of the emission region is randomly connected. These observations strongly imply that the central component of AGNs is likely a Supermassive Black Hole (SMBH), namely a rapidly accreting black hole.

AGN emissions span the entire electromagnetic spectrum [23], each wavelength band offers insights into specific components and associated phenomena within AGN.

In addition to the central SMBH [7] there is a disk of accreting matter onto it, that emits a significant amounts of ultraviolet (UV) radiation. Above this disk, a cloud of relativistic electrons is believed to be there [24].

This cloud reprocess the UV photons emitted from the disk, re-emitting them at X-ray energy levels. A population of clouds exists in close proximity to the SMBH, that is known as the Broad Line Region (BLR), because the kinematics of these clouds are significantly affected by the gravitational pull of the SMBH, resulting in broader spectral lines. Beyond the BLR, there exists an outer region surrounding the SMBH known as the Narrow Line Region (NLR). In contrast to the BLR, the NLR is characterized by narrower spectral lines, indicating distinct physical conditions and dynamics. Additionally, surrounding the disk, there's a toroidal-shaped volume composed of a mixture of gas and dust, leading to the partial absorption of central radiation.

The torus is the main component used from the "Unified Model" [25] to explain the existence of different populations of AGN.

Indeed, according to this model, different AGNs are the same population of objects with specific inclinations to our line-of-sight direction [26].

In particular we can distinguish:

- **Type I:** For these types of AGN, broad emission lines, emitted from the BLR, with typical width in the range of in the range of $\sim 10^3$-$10^4$km s$^{-1}$ exhibit a broad component, along with narrow emission lines from the NLR. In this configuration, the observer is situated at a small angle relative to the torus axis, allowing the radiation from circumnuclear regions to remain unobscured along the line of sight.

- **Type II:** In this scenario, the spectrum of the AGN comprises solely narrow emission lines, not exceeding 1200km s$^{-1}$, due to the fact that the line of sight intersects the obscuring matter of the torus, obscuring the BLR.

A visual overview can be found in Figure 1.1.

The energy released during the accretion process of a SMBH plays a significant role in shaping the evolution of the host galaxy [27]. In this context, the literature often discusses positive and negative feedback mechanisms. Positive feedback occurring when the AGN feedback promotes stellar formation, while negative feedback involves the suppression of star formation, respectively.

Feedback from SMBH accretion is capable of heating diffuse gas [28] and depositing heavy elements across the extensive surrounding environment

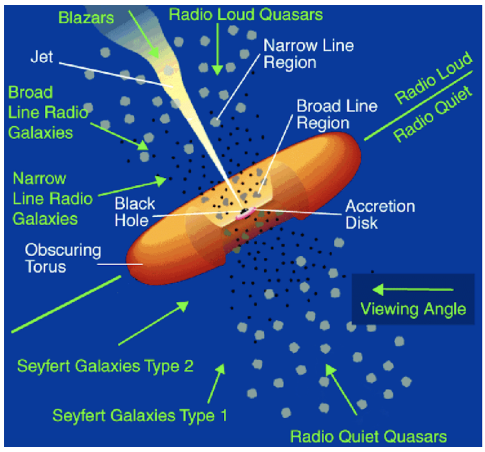


Figure 1.1: The Unified AGN model as proposed in [25]

[29], with effects observed at scales exceeding kpc scales.

Two distinct AGN feedback mechanisms have been proposed, each associated with different rates of mass accretion onto the SMBH (e.g. [30, 31]).

- **QSO's Radiative Feedback :** This feedback mode, often referred as quasar mode, consists in a high accretion rate of the SMBH via an optically-thick and geometrically-thin disk, and most of the energy is released in form of radiation.

- **QSO's Radio Feedback :** In this scenario, the SMBH accretion of hotter gas happens with a low rate in a optically-thin and geometrically-thick disk configuration, releasing energy in form of relativistic particles such as Radio Jets.

## 1.2 The Brightest Cluster Galaxies

The Hierarchical Galaxy Formation Model stands as a cornerstone in our understanding of cosmic structure formation, delineating the principal pathways through which galaxies growth their stellar and gas mass assimilating matter from their surroundings [32].

One of the most extreme examples in this context involves the study of Brightest Cluster Galaxies (BCGs), a unique class of galaxies, situated at the center and typically standing out as the most luminous and massive objects within the entire cluster.( e.g. [33] ).

Considering their environment, observational studies, such as [4], have indicated that the evolution of BCGs differs from the normal galactic path. The prevailing model for cosmic structure formation ( i.e. the Lambda Cold Dark Matter Model ΛCDM ) suggests that the mass assembly of BCGs is primarily influenced by dry mergers [5, 6].

BCGs, primarily elliptical galaxies, show unique luminosity profiles distinct from typical ellipticals outside clusters and generic bright galaxies. Their properties deviate from established scaling relations for ellipticals. While most BCGs align with the Fundamental Plane, deviations, such as lower velocity dispersions and larger radii than predicted by the Faber–Jackson and Kormendy relations, have been observed (e.g [34]). Recent findings suggest variations in these relations based on galaxy luminosity for all ellipticals. Additionally, BCG surface brightness profiles and radii depend on host cluster properties [35].

BCGs are mainly characterized by Radio Mode accretion of their SMBH, thus exhibiting radio loud emission as well as radio jets.

As presented in [11] these relativistic jets of radio emission are also recognized as one of the main explanation of the so called "Cooling flow problem". While Theoretical expectations propose rapid cooling and gas flow toward the center, fostering new star formation, actual observations reveal a much slower cooling process, leading to the discrepancies. The inclusion of radio jets provides a resolution to this issue by infusing energy into the Intracluster Medium (ICM), the hot gas within a galaxy cluster. This injection hinders the rapid cooling and collapse of gas toward the center, deviating from theoretical predictions.

However observational studies found that temperature of cluster cores fails to fall below $\sim 30\%$ at large radii resulting in an amount of cooling gas corresponding only to the $\sim 10\%$ expected from the existent cooling flow model. [36]

## 1.3 The Aim of this thesis

In this context, the main scientific question driving this work is to understand **whether the special evolution of BCGs, along with their dense environment, affects the accretion of SMBHs in their centers compared to other types of galaxies in the local universe**.

In particular, this study will present a comparative analysis between two representative samples of BCGs and Non-BCGs to highlight the substantial differences that the cluster environment induces in SMBH accretion.

To address this particular question, I conducted an analysis on a galaxy sample compiled from the Sloan Digital Sky Survey Data Release 7 (SDSS DR7), as outlined in [10], and the C4 BCGs catalogue created by [11]. For this specific BCG sample, I utilized the optical line fluxes ($H\alpha$, [OIII], $H\beta$, [NII], and [SII] doublets) provided by the Max Planck Institute for Astrophysics and Johns Hopkins University team to establish a comprehensive understanding of optical AGN presence through the [NII]- and [SII]- BPT diagnostic diagrams. Furthermore, through the cross-match between the aforementioned catalogs with datasets derived from NVSS and FIRST radio surveys, as outlined in [15], I identified BCGs associated with radio loud emission, as an indication of the presence of radio mode SMBH accretion and a potential radio jet.

These analyses, including data description and data analysis will be presented in the "Methods" chapter.

# Chapter 2

# Methods

In this thesis, I analyze a dataset comprising the properties of a sample of galaxies from the Seventh Data Release (DR7) of the Sloan Digital Sky Survey. Covering 11,663 square degrees of imaging data, DR7 offers extensive five-band photometry for 357 million celestial objects [10, 37].

With completed spectroscopy over 9380 square degrees, including 1.6 million spectra of galaxies, quasars, and stars, the SDSS DR7 dataset serves as the primary catalog for this study.

Specifically i will focus on following physical properties : **Redshift** and **Integrated flux with their relative uncertainties** of the common optical lines (i.e. $H\alpha$, $H\beta$...).

In the context of SDSS DR7, the line-fitting process is divided into three main stages during an automated Gaussian fitting procedure applied to continuum subtracted data as follows :

1. The first stage involves fitting to only emission lines, referred to as "foundLines," and is performed during the determination of emission line redshifts.

2. The second stage, termed "measuredLines," represents the final fitting of all lines, including both emission and absorption lines. This stage occurs after the object has been classified, and the redshift has been determined.

It is important to note that **each** line is **individually fitted as a single Gaussian** on the continuum-subtracted spectrum, with modalities shown in [13].

For the latter Radio identification i also use photometric informations, as later presented.

## 2.1 Data Description

This thesis presents results obtained through the cross-matching of three distinct celestial catalogues:

- **SDSS DR7 :** Our Main Catalogue of galaxies [10, 37]
- **C4-BCG :** The BCG Catalog [12]
- **Radio Emitters :** The survey chosen for RadioLoud identification [15]

### 2.1.1 SDSS DR7

The SDSS project, or Sloan Digital Sky Survey, is a comprehensive astronomical survey that maps the universe by capturing images, spectra, and photometric data of celestial objects over a large area of the sky, with a spectroscopic footprint area of 9'380 $deg^2$ and an imaging surface covered of 11'663 $deg^2$ [10] as shown in Figure 2.1.

Observations have been conducted using a a dedicated wide-field 2.5 m telescope [38] located at Apache Point Observatory (APO) near Sacramento Peak in Southern New Mexico.

The telescope employs two distinct instruments, making possible both Imaging and Spectroscopy measures.

Respectively, first measurements are carried out with a wide field imager composed by 24x 2048 × 2048 CCDs on the focal plane and described in [39]. This photometric system comprises five color bands (u, g, r, i, and z) that divide the entire range from the atmospheric UV cutoff at 3000 $\mathring{A}$ to the sensitivity limit of silicon CCDs at 11000 $\mathring{A}$ into five essentially non overlapping passbands.

The detection limit, defined at a Signal-to-Noise ratio (S/N) of 5, is approximately u' = 22.1 mag, g' = 23.2 mag, r' = 23.1 mag, i' = 22.5 mag, and z' = 20.8 mag for stars. Achieving a higher S/N of 50:1 (corresponding to photometry at the 2% level) occurs at magnitudes 19.1, 20.6, 20.4, 19.8, and 18.3 in the five bands, respectively. For typical galaxy images, the S/N

reaches half a magnitude to a magnitude brighter at the faint end, depending on their surface brightness. [39]

Rather than calculating the point-spread function (PSF) from scratch, the authors opted to synthesize the PSF for each point in the sky. This was achieved by taking a suitably weighted sum of the PSFs output by the SDSS photometric pipeline from each of the individual runs. [10].

On the other hand Spectroscopic Measurements are carried out with a pair of multiobject double spectrographs, receiving the light from 640 optical fiber. Targets of this subsequent measurements, are chosen based on previously captured photometric data, and arranged on tiles of $1\,^{\circ}49'$ with centers chosen to maximize the number of targeted objects as described in Blanton at Al. [40]

Each of the spectrographs cover a wavelength range from 3800 $\mathring{A}$ to 9200 $\mathring{A}$ with a spectral resolution of $\frac{\lambda}{\Delta\lambda} \approx 2000$. [10]

In this thesis, I work with a dataset of properties estimated by the Max Planck Institute for Astrophysics and Johns Hopkins University (MPA-JHU) team for a total of 927,552 galaxies belonging to the Sloan Digital Sky Survey Data Release 7 (SDSS DR7) [10, 37].

The main Physical Properties of Interest for our study, including **Redshift** and **Integrated flux with relative uncertainty** for common optical lines (i.e., $H\alpha$, $H\beta$) and molecular lines (i.e., [N II]6584, [O III]5007, [S II]6731, [S II]6716), are examined.

These properties resulted from calculations of two automated spectroscopic pipelines :*spectro2d* and *spectro1d* [41].

The *spectro2d* pipeline processes two-dimensional spectrograms from spectrographs, converting raw data and calibration images into merged, coadded, and calibrated spectra, along with noise estimates and mask arrays for subsequent analysis by the *spectro1d* pipeline.

The *spectro1d* pipeline classifies spectra, determines emission and absorption redshifts, and measures lines. It produces the specObj class containing parameters for the entire spectrum and related information, including flux- and wavelength-calibrated spectra and continuum-subtracted spectra.

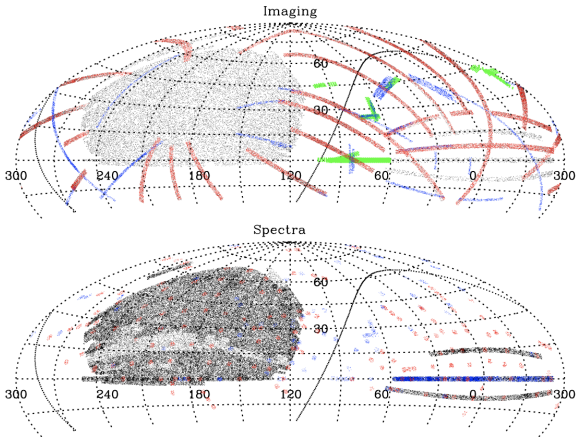


Figure 2.1: Regions of the sky surveyed by SDSS Data Release 7 [10]

### 2.1.2 C4 BCG Catalogue

The identification of BCGs within our primary galaxy sample, previously described, relies on the findings of A. Von der Linden et al. [11, 12]. These findings were derived from a subsequent analysis of the C4 Galaxy Cluster Catalog, initially developed by Miller et al. in 2005 [42].

The C4 catalog comprises 748 galaxy clusters identified in the Second Data Release (DR2) of the Sloan Digital Sky Survey (SDSS). Utilizing a seven-dimensional position and color space, the C4 cluster-finding algorithm identifies overdensities.

Covering approximately 2600 square degrees of the sky, the catalog spans redshifts from about 0.02 to 0.17. It includes various properties like sky location, mean redshift, galaxy membership, optical luminosity (Lr), velocity dispersion, and measures of substructure and large-scale environment.

This catalog represents one of the initial cluster catalogs constructed directly from SDSS spectroscopic data, addressing issues related to projection effects and employing mock galaxy catalogs derived from realistic N-body simulations to analyze the clustering algorithm's parameters and improve its completeness.

In this context, the work by Von Der Linden et al. [11] is noteworthy, as it builds upon the C4 catalog but introduces improved algorithms for BCG identification and measuring cluster velocity dispersion, ultimately yielding a sample of 625 BCGs.

Correcting for the SDSS photometric pipeline's tendency to underesti-

mate luminosities in dense environments, the research refines the C4 galaxy cluster sample, addressing issues related to BCG luminosity underestimation. Given the challenges with SDSS photometry, especially for large galaxies in crowded areas, the study avoids using magnitude measurements assuming a specific profile shape.

The C4 catalog provides potential BCG candidates, but approximately 30% of clusters miss the true BCG due to fiber collisions. To address this issue, Von der Linden's team developed an algorithm to identify the BCG by estimating the virial radius, selecting the two brightest galaxies within the mean galaxy's projection, and assessing criteria such as concentration index, color compatibility, and redshift.

### 2.1.3 The Radio Catalogue

To investigate the radio emission characteristics of both BCGs and non-BCGs, this study conducted a crossmatch between the primary SDSS sample and a dataset comprising 2,712 radio-luminous galaxies from the work by [15]. This collection of radio-luminous objects resulted from a complex cross-matching process involving the main spectroscopic galaxy sample and two radio surveys: the National Radio Astronomy Observatories (NRAO) Very Large Array (VLA) Sky Survey (NVSS) [16] and the Faint Images of the Radio Sky at Twenty centimeters (FIRST) survey. [17]

The NVSS was the first radio survey with a sufficiently high angular resolution (45 arcsec) to allow automated cross-correlation with optical surveys. However, the FIRST catalogue offers superior angular resolution (approximately 5 arcsec), resulting in samples with much higher reliability. Nonetheless, the high angular resolution of FIRST presents its own challenges, as it is insensitive to extended radio structures and resolves out the extended emission of radio sources. Consequently, the total radio luminosity of sources larger than a few arcseconds is systematically underestimated by FIRST. To address these limitations, a hybrid approach utilizing both NVSS and FIRST surveys has been developed to identify radio sources associated with galaxies in the SDSS spectroscopic sample. This approach capitalizes on the sensitivity of NVSS to large-scale radio structures and the high angular resolution of FIRST to reliably pinpoint the host galaxy.

The obtained radio source sample demonstrated a completeness of 95% and a reliability of 98.9%, upgrading the achievable performance of each

individual survey. The sample was subsequently classified into two groups: radio-loud active galactic nuclei (AGN) and galaxies where radio emission is predominantly driven by star formation. Classification was based on a galaxy's position in the 4000-Å break strength versus radio luminosity per unit stellar mass plane, resulting in a dataset of 2,215 radio-loud AGN and 497 star-forming galaxies with radio luminosity exceeding 5 mJy at 1.4 GHz.

## 2.2 Data Analysis

As previously introduced, our primary galaxy sample for astrometry measurements is the MPA-JHU SDSS-derived catalogue.

The first operation required for the development of our study involved crossmatching the C4 BCG sample [12] to extract data files from the main sample, including both BCGs and non-BCGs.

This initial crossmatch was accomplished by selecting the nearest element within a radius of 2 arcsec in both RA and Dec corresponding to each of the BCGs in [12]. The result was a list of 484 corresponding selected elements.

At the end of this initial phase, the following data were collected for both samples:

- **Astrometry data:** Celestial coordinates, Redshift, Error on redshift...
- **Spectroscopy measures:** Emission lines' fluxes and their relative errors

Even though further explanation is to follow, it is preferable to introduce the second crossmatch required for this work, this time with the 2712 galaxy samples of Celestial Objects found to be active in the radio field.

In this case, the research algorithm was designed to identify the nearest correspondence within a radius of 5 arcsec. The previously created files were appropriately updated by adding a specific flag, denoted as 1, to indicate whether, when found in the Radio Sample, it implies Radio Loud Emission.

### 2.2.1 Optical analysis

After previously introducing the defining properties of an AGN and discussing their effects on the host galaxy, it is crucial for the subsequent optical analysis of our two samples to examine which selected objects exhibit typical properties intrinsic to the presence of an AGN. One of the primary methods employed in Astrophysics is the analysis of BPT diagnostic diagrams [14].

This type of analysis classifies different species of galaxies by scrutinizing specific ratios of emission lines produced by ionizing gas in the galaxy's Interstellar Medium (ISM), utilizing photoionization models. These specific ratios have been carefully chosen to prioritize similar wavelength fractions,

minimizing dust attenuation. Specifically, this is developed based on the following ratios:

- $\frac{[OIII]\lambda 5007}{H\beta}$
- $\frac{[SII]\lambda\lambda 6716,6731}{H\alpha}$
- $\frac{[NII]\lambda 6583}{H\alpha}$
- $\frac{[OI]\lambda 6300}{H\alpha}$

By examining these ratios, which provide evidence of different photoionization models, it is possible to draw demarcation lines and ultimately classify the final objects into different categories.

The underlying concept of this method is rooted in an intrinsic property of the ionization spectrum of massive stars near the Lyman limit of Helium, found at $\lambda = 228\mathring{A}$. Massive stars exhibit a bright cut, while the non-thermal radiation of AGNs extends to higher energies.

As a result, AGN host galaxies typically show greater ratios that surpass the demarcation lines predicted by photoionization models.

There were several photoionization models at the inception of this technique; nowadays, the preferred ones are Kauffmann et al. [43] and Kewley et al. [44].

While the ideal classification incorporates all three primary BPT diagnostics, this study relies on a classification derived solely from the BPT diagrams for [NII] and [SII].

- **BPT-[NII] Demarcation Functions:**
  - Kauffmann+03 Line:

$$\log(\frac{\text{[OIII]}}{\text{H}\beta}) = 0.61/(\log(\frac{\text{[NII]}}{\text{H}\alpha}) - 0.05) + 1.3$$

  - Kewley+01 Line:

$$\log(\frac{\text{[OIII]}}{\text{H}\beta}) = 0.61/(\log(\frac{\text{[NII]}}{\text{H}\alpha}) - 0.47) + 1.19$$

- **BPT-[SII] Demarcation Functions:**
  - Main AGN Line:

$$\log(\frac{\text{[OIII]}}{\text{H}\beta}) = 0.72/(\log(\frac{\text{[SII]}}{\text{H}\alpha}) - 0.32) + 1.30$$

– LINER/Sy2 Line:

$$\log(\frac{[\text{OIII}]}{\text{H}\beta}) = 1.89\log(\frac{[\text{SII}]}{\text{H}\alpha}) + 0.76$$

As follows it is presented a brief description of each population:

- **BPT-[NII]:**
  - **Star-forming (SF):** Below both of the demarcation lines, where the ionization is primarily from massive stars.
  - **AGN (Active Galactic Nuclei):** Above both of the demarcation lines, delineating ionization by an active nucleus.
  - **Composite:** Galaxies exhibiting a mix of both star-forming and AGN characteristics. Generally recognized to be in the area between both of the demarcation lines.
- **BPT-[SII]:**
  - **Seyferts:** Above of both of the demarcation lines, characterized by high ionization levels.
  - **LINERs (Low-Ionization Nuclear Emission Regions):** Above the Main AGN line, and below LINER/Sy2. Typically characterized by weak AGN-like ionization.
  - **Star-forming HII2:** Galaxies exhibiting ionization characteristics similar to HII regions in star-forming galaxies.

Returning to the methodology employed in this thesis, an initial screening process was conducted to exclude objects with flux values that rendered logarithmic ratios incalculable, specifically eliminating instances with numerators or denominators equal to zero. Subsequently, scatterplots were generated and demarcation lines were applied to discern distinct galaxy populations. Results images can be seen in :

Figure 2.2 Figure 2.3 Figure 2.4 Figure 2.5

Given the inclusion of error values for each flux measurement, a robust bootstrap algorithm was implemented through 5000 iterations. This algorithm introduced variations to each point on the diagnostic diagram in two

dimensions based on its probability distribution, with the mean value reflecting the error-free point and a standard deviation equivalent to the error associated with the point in both directions.

This rigorous approach facilitated an accurate determination of counts and fractions for all populations, providing a statistically refined measure of uncertainty.

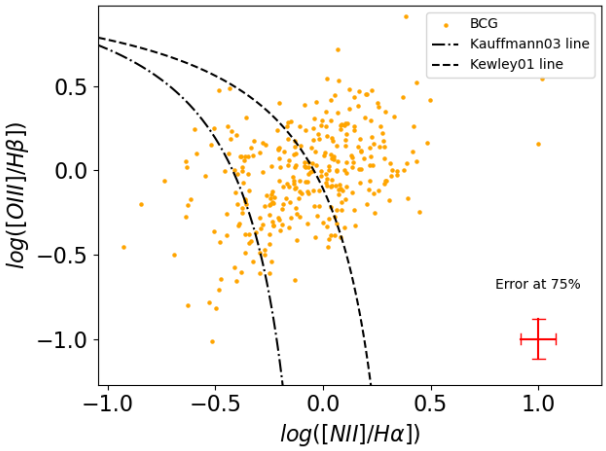


Figure 2.2: BPT NII for the BCG sample

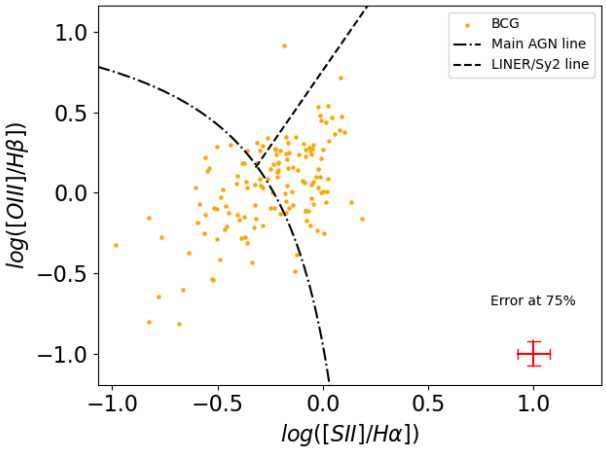


Figure 2.3: BPT SII for the BCG sample

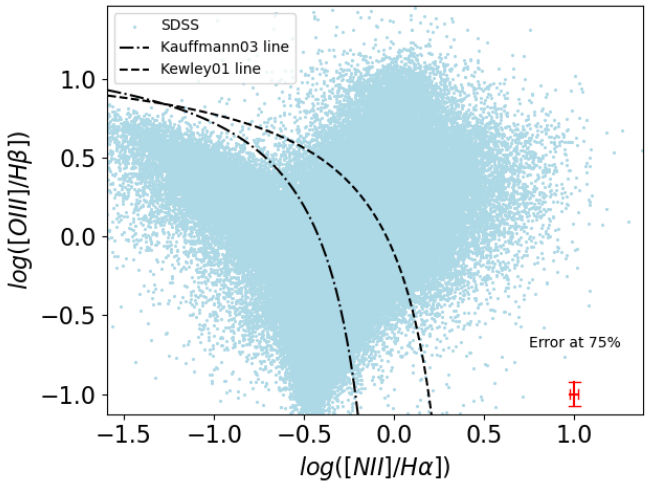


Figure 2.4: BPT NII for the SDSS noBCG sample

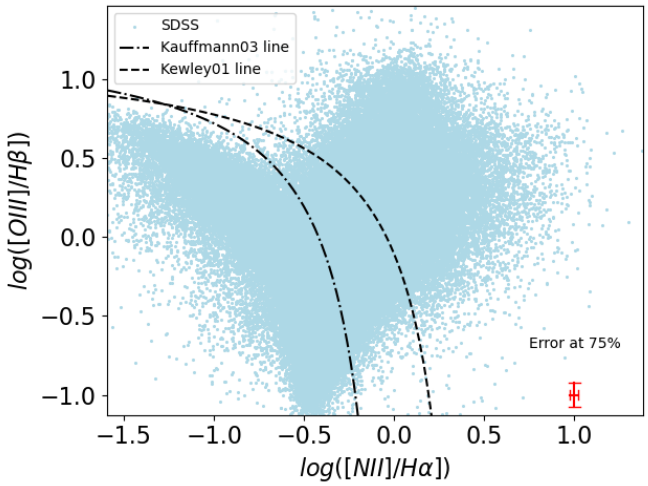


Figure 2.5: BPT SII for the SDSS noBCG sample

### 2.2.2 Radio Analysis

Following the preceding analyses, let's now detail how the fractions of Radio Loud AGNs were calculated for the two derived samples.

The primary goal of this analysis segment is to determine a fraction of the form :

$$\frac{N_{\text{radio}}}{N_{\text{total}}}$$

A crucial step in calculating a representative fraction of Radio Loud objects was to appropriately define the spatial regions for the fraction calculations. To accomplish this, we identified the regions mapped by the radio survey employed. Subsequently, the selection has been delineated where all three catalogs exhibited an overlap. It is essential to emphasize that the primary objective is to obtain representative fractions for both of our samples.

The selected spatial regions considered for calculating the fractions of Radio Loud objects can be found in Figure 2.6

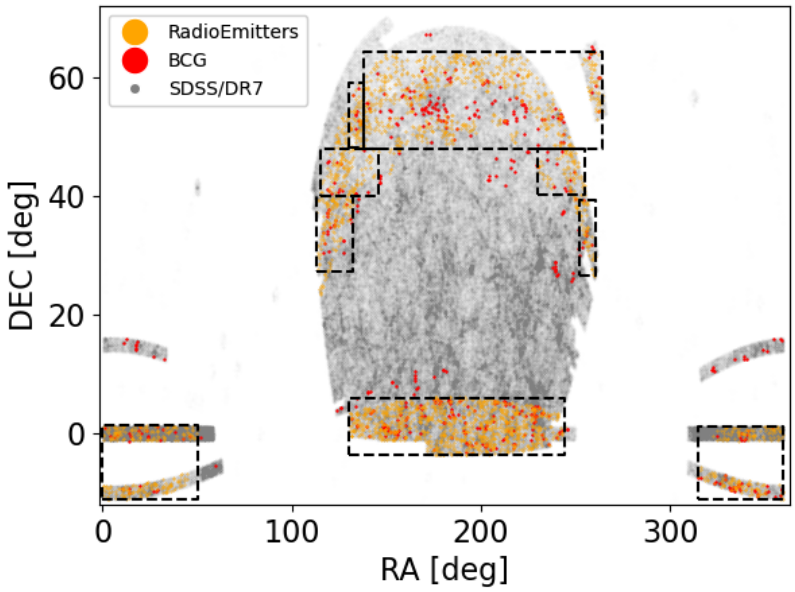


Figure 2.6: Defining Regions of Radio Loud AGN fractions

# Chapter 3

# Results

At the conclusion of the analysis, a comparison between the results obtained in the two samples was conducted, and the outcomes are presented in the following tables.

In Table 3.1, detailing the results of the optical analysis, it is observed that BCGs are more likely to host an AGN compared to ordinary galaxies. These findings align with those presented in the work of Vitale et al. [18], where the analysis was based on a statistically larger sample than the one employed in this study.

| Diagram | Spectral Type | SDSS DR7 subsample | Crossmatch C4-BCG |
|---|---|---|---|
| [NII] | AGNs | $52896 \pm 84$ $(21.1 \pm 0.03)\%$ | $161 \pm 5$ $(50.4 \pm 1.6)\%$ |
| | Composites | $55875 \pm 110$ $(22.3 \pm 0.04)\%$ | $110 \pm 5$ $(34.5 \pm 1.8)\%$ |
| | SFGs | $141753 \pm 80$ $(56.6 \pm 0.03)\%$ | $49 \pm 4$ $(15.4 \pm 1.4)\%$ |
| [SII] | Seyferts | $13082 \pm 64$ $(6.3 \pm 0.03)\%$ | $8 \pm 2$ $(6.5 \pm 1.6)\%$ |
| | LINERs | $28396 \pm 80$ $(13.6 \pm 0.04)\%$ | $74 \pm 3$ $(53.3 \pm 2.4)\%$ |
| | SFGs | $167826 \pm 76$ $(80.2 \pm 0.04)\%$ | $55 \pm 3$ $(40.2 \pm 2.2)\%$ |

Table 3.1: Results of the optical analysis

Simultaneously, the analysis of Radio Loud emissions indicates that BCGs are more likely to host Radio Loud Activity, with a fraction of 12%. This value is 20 times higher than the fraction found for the non-BCG subsample of galaxies within the selected regions, as discussed earlier, corresponding to 0.6%.

# Conclusions

The evolutionary processes of BCGs are still not fully understood, and there are no specific studies comparing the frequency of different types of AGN in BCGs with respect to other types of galaxies (e.g., [9]).

The central inquiry driving this thesis project is: *Does the unique evolutionary path of BCGs, shaped by their distinctive environmental conditions, contribute to heightened SMBH accretion at their cores compared to other galaxy types in the local universe?*

To tackle this scientific inquiry, this study conducts a comparative analysis on samples of Brightest Cluster Galaxies (BCGs) and non-BCGs. The samples are derived through the cross-matching of three distinct celestial catalogs, encompassing a comprehensive galaxy sample[10], a specific BCG sample [12], and a radio survey identifying objects with pronounced radio emission [15].

The analysis we carried out produced the following results:

1. BCGs show greater AGN activity than ordinary galaxies.

2. The unique environmental conditions within the cluster play a crucial role in shaping the distinctive form of AGN feedback. The preference for shock-induced gas interactions through radio jets is evident, leading to a higher percentage of Low-Ionization Nuclear Emission-line Region (LINER) phenomena compared to Seyfert galaxies.

3. In support of the preceding observation, the BCG sample exhibits a radio loudness fraction that is 20 times higher, providing further confirmation.

Future enhancements to the methodology outlined in this study could involve incorporating a galaxy selection based also on mass magnitude.

# Bibliography


[1] A. Sandage and Kristian. The extension of the Hubble diagram. I. New redshifts and BVR photometry of remote cluster galaxies, and an improved richness correction. *The Astrophysical Journal*, 205:688–695, May 1976. doi: 10.1086/154324.

[2] Anja von der Linden and Wild. Star formation and AGN activity in SDSS cluster galaxies. *Monthly Notices of the Royal Astronomical Society*, 404(3):1231–1246, May 2010. doi: 10.1111/j.1365-2966.2010.16375.x.

[3] Danièl N. Groenewald and Skelton. The close pair fraction of BCGs since z = 0.5: major mergers dominate recent BCG stellar mass growth. *Monthly Notices of the Royal Astronomical Society*, 467(4):4101–4117, June 2017. doi: 10.1093/mnras/stx340.

[4] A. Travascio and Bongiorno. Multiple AGN activity during the BCG assembly of XDCPJ0044.0-2033 at z $\sim$ 1.6. *Monthly Notices of the Royal Astronomical Society*, 498(2):2719–2733, October 2020. doi: 10.1093/mnras/staa2495.

[5] Gabriella De Lucia and Jérémy Blaizot. The hierarchical formation of the brightest cluster galaxies. *Monthly Notices of the Royal Astronomical Society*, 375(1):2–14, February 2007. doi: 10.1111/j.1365-2966.2006.11287.x.

[6] Kevin C. Cooke and Kartaltepe. Stellar Mass Growth of Brightest Cluster Galaxy Progenitors in COSMOS Since z $\sim$ 3. *The Astrophysical Journal*, 881(2):150, August 2019. doi: 10.3847/1538-4357/ab30c9.

[7] D. A. Rafferty and McNamara. The Feedback-regulated Growth of Black Holes and Bulges through Gas Accretion and Starbursts in Clus-

ter Central Dominant Galaxies. *The Astrophysical Journal*, 652(1): 216–231, November 2006. doi: 10.1086/507672.

[8] John P. Stott and Hickox. The XMM Cluster Survey: the interplay between the brightest cluster galaxy and the intracluster medium via AGN feedback. *Monthly Notices of the Royal Astronomical Society*, 422 (3):2213–2229, May 2012. doi: 10.1111/j.1365-2966.2012.20764.x.

[9] S. Fisek and Alis. AGN Activity in Brigtest Cluster Galaxies (BCGs). *Communications of the Byurakan Astrophysical Observatory*, 66(2): 153–158, December 2019. doi: 10.52526/25792776-2019.66.2-153.

[10] Kevork N. Abazajian and Adelman-McCarthy. The Seventh Data Release of the Sloan Digital Sky Survey. *Astrophysical Journal Supplement Series*, 182(2):543–558, June 2009. doi: 10.1088/0067-0049/182/2/543.

[11] Anja Von Der Linden and Best. How special are brightest group and cluster galaxies? *Monthly Notices of the Royal Astronomical Society*, 379(3):867–893, August 2007. doi: 10.1111/j.1365-2966.2007.11940.x.

[12] A. von der Linden and Best. VizieR Online Data Catalog: BCG C4 cluster catalog (von der Linden+, 2007). VizieR On-line Data Catalog: J/MNRAS/379/867. Originally published in: 2007MNRAS.379..867V, July 2009.

[13] James E. O'Donnell. R v-dependent Optical and Near-Ultraviolet Extinction. *The Astrophysical Journal*, 422:158, February 1994. doi: 10.1086/173713.

[14] J. A. Baldwin, M. M. Phillips, and R. Terlevich. Classification parameters for the emission-line spectra of extragalactic objects. *Publications of the Astronomical Society of the Pacific*, 93:5–19, February 1981. doi: 10.1086/130766.

[15] P. N. Best, G. Kauffmann, T. M. Heckman, and Ž. Ivezić. A sample of radio-loud active galactic nuclei in the Sloan Digital Sky Survey. *Monthly Notices of the Royal Astronomical Society*, 362(1):9–24, September 2005. doi: 10.1111/j.1365-2966.2005.09283.x.

[16] J. J. Condon and Cotton. The NRAO VLA Sky Survey. *The Astronomical Journal*, 115(5):1693–1716, May 1998. doi: 10.1086/300337.

[17] Robert H. Becker and White. The FIRST Survey: Faint Images of the Radio Sky at Twenty Centimeters. *The Astrophysical Journal*, 450:559, September 1995. doi: 10.1086/176166.

[18] M. Vitale and Zuther. Classifying radio emitters from the Sloan Digital Sky Survey. Spectroscopy and diagnostics. *Astronomy & Astrophysics*, 546:A17, October 2012. doi: 10.1051/0004-6361/201219290.

[19] Z. S. Yuan, J. L. Han, and Z. L. Wen. Radio luminosity function of brightest cluster galaxies. *Monthly Notices of the Royal Astronomical Society*, 460(4):3669–3678, August 2016. doi: 10.1093/mnras/stw1125.

[20] P. Oliva-Altamirano and Brough. Galaxy And Mass Assembly (GAMA): testing galaxy formation models through the most massive galaxies in the Universe. *Monthly Notices of the Royal Astronomical Society*, 440(1):762–775, May 2014. doi: 10.1093/mnras/stu277.

[21] Gregory A. Shields. A brief history of active galactic nuclei. *Publications of the Astronomical Society of the Pacific*, 111(760):661, jun 1999. doi: 10.1086/316378. URL `https://dx.doi.org/10.1086/316378`.

[22] L. Woltjer. Emission Nuclei in Galaxies. *The Astrophysical Journal*, 130:38, July 1959. doi: 10.1086/146694.

[23] Paolo Padovani. On the two main classes of active galactic nuclei. *Nature Astronomy*, 1:0194, August 2017. doi: 10.1038/s41550-017-0194.

[24] M. Kishimoto, R. Antonucci, C. Boisson, and O. Blaes. Revealing AGN by Polarimetry. In A. Adamson, C. Aspin, C. Davis, and T. Fujiyoshi, editors, *Astronomical Polarimetry: Current Status and Future Directions*, volume 343 of *Astronomical Society of the Pacific Conference Series*, page 435, December 2005. doi: 10.48550/arXiv.astro-ph/0408106.

[25] C. Megan Urry and Paolo Padovani. Unified Schemes for Radio-Loud Active Galactic Nuclei. *Publications of the Astronomical Society of the Pacific*, 107:803, September 1995. doi: 10.1086/133630.

[26] Robert Antonucci. Unified models for active galactic nuclei and quasars. *Annual Review of Astronomy and Astrophysics*, 31:473–521, January 1993. doi: 10.1146/annurev.aa.31.090193.002353.

[27] V. A. Masoura and Mountrichas. Relation between AGN type and host galaxy properties. *Astronomy & Astrophysics*, 646:A167, February 2021. doi: 10.1051/0004-6361/202039238.

[28] Tiziana Di Matteo and Springel. Energy input from quasars regulates the growth and activity of black holes and their host galaxies. *Nature*, 433(7026):604–607, February 2005. doi: 10.1038/nature03335.

[29] Karl Gebhardt and Bender. A Relationship between Nuclear Black Hole Mass and Galaxy Velocity Dispersion. *Astrophysical Journal Letters*, 539(1):L13–L16, August 2000. doi: 10.1086/312840.

[30] A. C. Fabian. Observational Evidence of Active Galactic Nuclei Feedback. *Annual Review of Astronomy and Astrophysics*, 50:455–489, September 2012. doi: 10.1146/annurev-astro-081811-125521.

[31] C. M. Harrison. Impact of supermassive black hole growth on star formation. *Nature Astronomy*, 1:0165, July 2017. doi: 10.1038/s41550-017-0165.

[32] S. Cole, A. Aragon-Salamanca, C. S. Frenk, J. F. Navarro, and S. E. Zepf. A recipe for galaxy formation. *Monthly Notices of the Royal Astronomical Society*, 271:781–806, December 1994. doi: 10.1093/mnras/271.4.781.

[33] Z. L. Wen and J. L. Han. Dependence of the bright end of composite galaxy luminosity functions on cluster dynamical states. *Monthly Notices of the Royal Astronomical Society*, 448(1):2–8, March 2015. doi: 10.1093/mnras/stu2722.

[34] William R. Oegerle and John G. Hoessel. Fundamental Parameters of Brightest Cluster Galaxies. *The Astrophysical Journal*, 375:15, July 1991. doi: 10.1086/170165.

[35] S. Brough, C. A. Collins, D. J. Burke, P. D. Lynam, and R. G. Mann. Environmental dependence of the structure of brightest cluster galaxies. *Monthly Notices of the Royal Astronomical Society*, 364(4):1354–1362, December 2005. doi: 10.1111/j.1365-2966.2005.09679.x.

[36] L. P. David, P. E. J. Nulsen, B. R. McNamara, W. Forman, C. Jones, T. Ponman, B. Robertson, and M. Wise. A high-resolution study of the

hydra a cluster with chandra: Comparison of the core mass distribution with theoretical predictions and evidence for feedback in the cooling flow. *The Astrophysical Journal*, 557(2):546, aug 2001. doi: 10.1086/322250. URL `https://dx.doi.org/10.1086/322250`.

[37] Max-Planck-Institut für Astrophysik. Sdss data release 7, s.d. URL `https://wwwmpa.mpa-garching.mpg.de/SDSS/DR7/`. Accesso in data: March 7, 2024.

[38] Gunn. The 2.5 m Telescope of the Sloan Digital Sky Survey. *The Astronomical Journal*, 131(4):2332–2359, April 2006. doi: 10.1086/500975.

[39] Gunn. The Sloan Digital Sky Survey Photometric Camera. *The Astronomical Journal*, 116(6):3040–3081, December 1998. doi: 10.1086/300645.

[40] Blanton. An Efficient Targeting Strategy for Multiobject Spectrograph Surveys: the Sloan Digital Sky Survey "Tiling" Algorithm. *The Astronomical Journal*, 125(4):2276–2286, April 2003. doi: 10.1086/344761.

[41] Stoughton. Sloan Digital Sky Survey: Early Data Release. *The Astronomical Journal*, 123(1):485–548, January 2002. doi: 10.1086/324741.

[42] Christopher J. Miller and Nichol. The C4 Clustering Algorithm: Clusters of Galaxies in the Sloan Digital Sky Survey. *The Astronomical Journal*, 130(3):968–1001, September 2005. doi: 10.1086/431357.

[43] Guinevere Kauffmann and Heckman. The host galaxies of active galactic nuclei. *Monthly Notices of the Royal Astronomical Society*, 346(4):1055–1077, December 2003. doi: 10.1111/j.1365-2966.2003.07154.x.

[44] L. J. Kewley and Dopita. Theoretical Modeling of Starburst Galaxies. *The Astrophysical Journal*, 556(1):121–140, July 2001. doi: 10.1086/321545.